THE JOURNAL OF PHYSICAL CHEMISTRY A

ARTICLE

pubs.acs.org/JPCA

Transition Dipole Moments of the Q_y Band in Photosynthetic Pigments

M. Belén Oviedo and Cristián G. Sánchez*

Departamento de Matemática y Física, Facultad de Ciencias Químicas, INFIQC, Universidad Nacional de Córdoba, Ciudad Universitaria, X5000HUA Córdoba, Argentina

ABSTRACT: From studying the time evolution of the single electron density matrix within a density functional tight-binding formalism we calculate the Q_y transition dipole moments vector direction and strength for a series of important photosynthetic pigments. We obtain good agreement with first-principles and experimental results and provide insights into the detailed nature of these excitations from the time evolving populations of molecular orbitals involved as well as correlations between pigment chemistry and dipole strength.

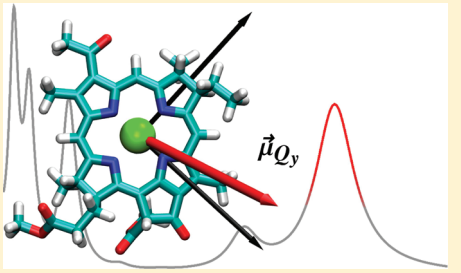

INTRODUCTION

Photosynthesis represents the main source of energy sustaining life on earth. The primary process of photosynthesis starts with the absorption of sunlight by an arrangement of photosynthetic pigments embedded into a proteic matrix called the light harvesting (LH) antenna complexes. The excitation energy of photosynthetic pigments is then transferred to the photosynthetic reaction center where it is converted into chemical energy. The primary process of photosynthesis occurs with a quantum yield close to unity[1] and recent experimental evidence suggests that this high efficiency can be due to suppression of environmental decoherence of excitons within antenna complexes.[2,3] Up to now there is no finished theoretical picture about the energy transfer process that can include all relevant factors into account. Several theoretical approaches have been applied to study this phenomenon, most of which are based on parametrized Hamiltonians containing information about the interchromophore couplings and the excitation energy of individual pigments embedded in their proteic environment. Most of these parameters are obtained from experimental data,[4−7] but it would be highly desirable to have alternate theoretical tools that can provide reliable information on pigment excitation to contrast with experimental data and provide an atomistic picture of the process that can cover the scale going from individual pigments to arrangements of pigments embedded in their native protein environment. The aim of this work is to take the first step in this direction.

Most photosynthetics pigments are chlorophylls (Chl), bacteriochlorophylls (BChl), and carotenoids, they represent the keystone for energy storage in photosynthetic organisms.[1] Figure 1a shows a generic chlorophyll molecule, where the structure of the porphyrin ring and the numbering of carbon atoms are depicted. Figure 1b displays the main axes of the molecule. By convention, the *y* molecular axis of chlorophylls and bacteriochlorophylls is defined as the axis passing through the N atoms of rings A and C;[1] here we define the *x* molecular axis as that perpendicular to the *y* axis that passes through the N atom of ring B. The *z* molecular axis is taken to be perpendicular to the *xy* plane.

In a previous publication, we studied the optical absorption as well as the energy transfer of a dimer of chlorophylls from an atomistic model.[8] The spectrum of photosynthetic pigments exhibits essentially two characteristic absorption bands (Figure 2): one of them called the Soret band can be found in the UV region and is a complex band composed of a large series of electronic transitions. The other called Q is in the visible region of the spectrum and is the most important for the photophysics involved in the photosynthetic process. This band can usually be decomposed in two distinct bands called Q_x and Q_y according to their predominant polarization; there is agreement that most of the energy absorbed by photosynthetic organisms comes from excitation of excitonically coupled Q bands of chlorophyll arrangements within antenna complexes.[1] As shown in ref 8, our method provides an excellent description of the absorption spectrum of all of the studied pigments with an absolute error that is smaller than the results obtained from full TDDFT calculations; this is probably due to a cancellation of errors in the approximate description provided by DFTB, with the advantage that large systems can be studied affordably. This cancellation comes from the truncation of the second-order expansion of the self-consistent terms in the Hamiltonian, which forces long-range interactions between charge fluctuations to be of Coulomb type. Furthermore, the truncation of long-range matrix elements in the non-self-consistent Hamiltonian restricts charge transfer excitations between fragments that are separated by more than the cutoff distance. These are clearly approximations

Received: April 25, 2011
Revised: October 3, 2011
Published: October 04, 2011

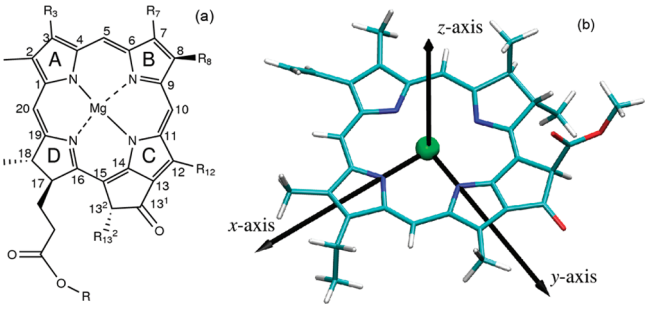

Figure 1. (a) Generic molecular model of chlorophyll showing the structure of the porphyrinic ring and the numbering of carbon atoms within it. For the calculations described in the text the phytyl chain in all cases has been replaced by a hydrogen atom. (b) Chlorophyll *a* molecular model showing the main molecular axes and the transition dipole vector of the Q_y band.

within TD-DFTB. However, these approximations allow a better description of excited states (at least in this sense) than its parent TD-DFT method.

Besides the absorption energy, the Q_y transition dipole moment is an important parameter for studying the mechanism of energy transfer, the simulations of optical spectra and calculations of excitonic couplings in antenna complexes. It is crucial for the calculation of coupling terms between pigments that are an integral part of model Hamiltonians. Therefore, it is very important to have precise knowledge of the magnitude and direction of the transition dipole moment vector as a starting point for models of light harvesting complexes. In a completely symmetric and unsubstituted tetraporphyrin, the transition dipoles moments for Q_x and Q_y bands are aligned with the molecular axes.[9] Natural photosynthetic pigments are highly asymmetric and have a variety of chemical modifications that change the polarization directions from their ideal orientation. Recent studies involving femtosecond visible pump infrared probe experiments revealed that the dipole moment corresponding to the Q_y band of Chla is about 12° away from the *y* molecular axis measured counterclockwise.[10,11] The complete determination of the dipolar strength and its orientation is a difficult task which requires input from theoretical data.[10]

In this paper we study the full dynamical evolution of the one electron density matrix within a DFTB (density functional tight binding) Hamiltonian in response to different kinds of external time-dependent electric fields. From this simulation we obtain the electronic transition dipole moments and their orientations for a series of chlorophylls and bacteriochlorophylls. The results obtained are compared with first principles (obtained from time dependent density functional theory) and experimental results found in the literature and analyzed in terms of the chemical structure of the pigment.

■ COMPUTATIONAL METHOD

The description of the electronic structure of photosynthetic pigments was carried out using the self-consistent density functional tight-binding (SCC-DFTB) method. This method has been successfully used for the calculation of the electronic structure of large molecular systems.[12] It is based on the second-order expansion of the Kohn−Sham energy functional around a reference density composed of neutral atomic species. The DFTB+ code is a sparse matrix implementation of the

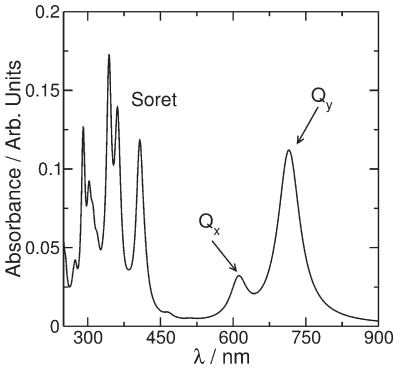

Figure 2. Absorption spectra of BChl *a*. The characteristic absorption bands are depicted.

DFTB method. We have used this code to obtain the Hamiltonian, the overlap matrix, and the ground state single electron density matrix. The methodology used in this work to obtain the optical properties of the system is based on the time propagation of the one electron density matrix after an initial perturbation is applied. For further details on the method and its validation for the description of absorption spectra of chlorophylls refer to Oviedo et al.[8] All molecular geometries of the photosynthetic pigments studied were fully optimized within the DFTB framework and correspond to those previously published in ref 8.

For the calculation of absorption spectra, we apply an initial perturbation in the shape of a Dirac delta ($\hat{H} = \hat{H}_0 + E_0\delta(t - t_0)\hat{\mu}$) to the initial ground state density matrix obtained from DFTB +.[13] After the pulse application, the density matrix evolves in time and its evolution can be calculated by integrating the Liouville−Von Neumann equation of motion in the nonorthogonal atomic orbital basis:

$$\frac{\partial\hat{\rho}}{\partial t} = \frac{1}{i\hbar}(S^{-1}\hat{H}[\hat{\rho}]\hat{\rho} - \hat{\rho}\hat{H}[\hat{\rho}]S^{-1}) \quad (1)$$

where S^{-1} is the inverse of the overlap matrix. Within the linear response regime, when the applied electric field is small, the response is linear and the dipole moment corresponds to

$$\mu(t) = \int_{-\infty}^{\infty} \alpha(t-\tau)\ E(\tau)\ d\tau \quad (2)$$

where $\alpha(t - \tau)$ is the polarizability along the axis over which the external field $E(t)$ is applied. The absorption spectrum is proportional to the imaginary part of the frequency dependent polarizability, obtained from the Fourier transform of the time-dependent dipole moment, after the deconvolution of the applied electric field ($E(t) = E_0\delta(t_0 - t)$ with E_0 = 0.001 V/Å in all cases):

$$\alpha(\omega) = \frac{\mu(\omega)}{E_0} \quad (3)$$

To make the dipole signal die out within the simulated time window, an exponential damping with a time constant of 10 fs is applied before transforming to frequency space, uniformly broadening all of the spectral lines. The average polarizability along the three Cartesian axes is taken as the absorption spectrum of the system. We have checked that the spectrum is independent of the magnitude of the initially applied field, indicating that the simulations are performed within the linear response regime where the time-dependent polarizability may be

Table 1. Angles of the Q_y Transition Vector for Different Photosynthetic Pigments[a]

molecule	θ	ϕ
BChla	92.9	1.4
BChlb	93.4	7.0
Chld	91.3	4.9
Chla	91.5	−2.3
BChld	86.9	−1.2
BChlc	88.2	0.6
Chlb	90.3	−0.9
BChle	91.0	3.3

[a] ϕ is the counterclockwise measured angle between the transition dipole moment and the y molecular axis; θ is the angle formed by the transition dipole moment and the z molecular axis. See Figure 3.

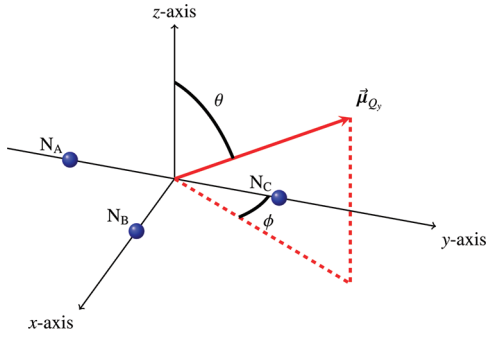

Figure 3. Scheme that displays the direction of the dipole moment in spherical coordinates. N_i is the nitrogen atom corresponding to the ith ring. ϕ is the azimuthal angle of its orthogonal projection on the xy plane, θ is the polar angle. μ_{Q_y} is the magnitude of the transition dipole moment.

extracted from the response using equation (eq 3). The full polarizability tensor at all frequencies can be obtained from three independent simulations in which the initial field is applied in three mutually orthogonal directions.[14]

RESULTS AND DISCUSSION

It is known that the Q_y transition dipole moment vector for Chla (chlorophyll a) deviates slightly from the y molecular axis. This has been demonstrated both experimentally[9−11,15,16] and theoretically.[17] The angle of the Q_y transition dipole moment measured from the y molecular axis for Chla ranges from +26° to −7°.[9−11,15−17] The great variation between these results relates to the different environments of Chla in different experimental situations. These small deviations of the Q_y transition vector have only a small effect on the properties of the absorption spectrum.

To obtain the direction of the Q_y transition dipole vector, we calculate the second rank polarizability tensor $\overleftrightarrow{\alpha}(\lambda_0)$, as described above, where λ_0 is the wavelength of the transition Q_y. After diagonalizing this tensor, the corresponding eigenvector having the largest eigenvalue can be associated with the direction where the transition occurs.

Table 1 shows θ and ϕ angles, corresponding to the spherical coordinates, of the Q_y transition dipole moment. It is noted that for chlorophylls and the BChle molecule the vector is only slightly shifted off the molecular plane, θ being close to 90°,

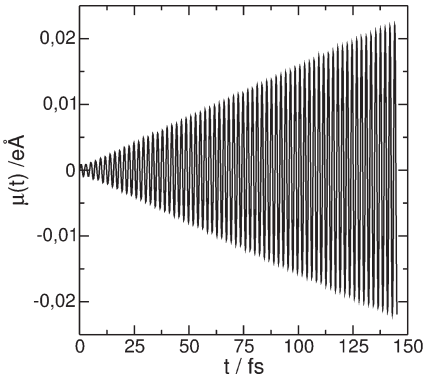

Figure 4. Time dependent variation of the dipole moment of a chlorophyll a molecule in response to laser illumination. The field intensity was 0.0001 V/Å and $\hbar\omega_{Q_y}$ = 1.9 eV.[8]

whereas bacteriochlorophylls have their dipole moment farther away from the molecular plane. The shift of the vector from the plane can be related to the chemical structure. Because the porphyrin ring is only partially reduced on Chl's and BChle molecules, this leads to an increase of the conjugation of the π system, making the transition closer to the one that would be obtained for a perfect porphyrin. On the other hand, we observe that the transition dipole moment is slightly shifted off of the y molecular axis, the largest deviation is observed for bacteriochlorophyll b and chlorophyll d.

Figure 4 shows the variation of the dipole moment in time for Chla, when we apply laser illumination in tune with the molecule Q_y excitation ($E(t) = E_0 \sin(\omega_{Q_y} t)$). We can see that the dipole moment oscillation amplitude grows linearly with time, as can be expected for an applied field within the linear response regime and in the absence of any dissipative mechanism.

If we model each photosynthetic pigment as a two level system (TLS), where the energy difference between the levels is equal to the energy of the Q_y transition, then the full quantum response function for our model is[18]

$$\alpha(t-\tau) = \frac{2}{\hbar}\theta(t-\tau)|\mu_{Q_y}|^2 \sin(\omega_{Q_y}(t-\tau)) \quad (4)$$

where $\theta(t-\tau)$ is the step function, $|\mu_{Q_y}|^2$ is the electronic transition dipole moment, and ω_{Q_y} is the transition frequency. Substituting (eq 4) in equation (eq 2) and by applying a monochromatic electric field polarized in the direction of the transition Q_y the value of the dipole moment for long times can be approximated by

$$\mu(t) \simeq \frac{E_0}{\hbar}|\mu_{Q_y}|^2 t \cos(\omega_{Q_y} t) \quad (5)$$

We can see from eq 5 that the oscillation amplitude has a linear dependence on time. To obtain the value of the Q_y transition dipole moment, we fit the local extrema of all oscillations of the calculated dipole moment to a linear function and obtain the transition dipole moment from its slope. The dipole strength can also be obtained from the diagonalization of the polarizability tensor obtained from an initial delta excitation as done for its direction. However, using the dipole signal from an in-tune laser excitation provides confirmation of the determination of its direction from the absence of precession, and we find it more reliable because no deconvolution and damping is necessary and the result comes right out of the time dependent signal.

Table 2. Comparison of Transition Dipole Moments Values, $|\mu_{Q_y}|^2$ (Debye^2), of Different Photosynthetic Pigments in Vacuum Obtained by the Method Described in the Text and ab Initio TD-DFT Results, with Experimental Values Find in the Literature[19,20]

molecule	$\|\mu_{Q_y}\|^2$ (TD-DFTB)	$\|\mu_{Q_y}\|^2$ (TD-DFT)	experiment value
BChla	44.2	53.2	37.1
BChlb	36.6	48.6	
Chld	25.0	31.4	
Chla	23.8	29.6	21.0
BChld	19.0	24.6	
BChlc	17.9	23.7	(20.3 − 34.3)
Chlb	16.5	20.8	14.7
BChle	7.4	13.2	

Table 2 shows the values of the transition dipole moment for different photosynthetic pigments in vacuum. We compare the results obtained by TD-DFTB calculations with those obtained by TD-DFT,[†] and also with experimental data found in the literature. Experimental values of the transition dipole moment in vacuum for BChla, Chla, and Chlb were determined from an *empty cavity* analysis[19,20] starting from spectroscopic data of the pigments in different solvents and extrapolating to the vacuum value using a model for the influence of the solvent. The transition dipole moment for BChlc is an average between experimental values obtained in different solvents and is not corrected for the presence of solvent.[20] These are the only values we have found in the literature for the transition dipole moments in vacuum and therefore the ones that are more comparable to the results of our calculations. For the BChlb molecule in ether the value found is of 50 D^2 [22] and for the Chld molecule it is of 25 D^2, where the latter is obtained for the pigment bound to a water-soluble protein.[23] Figure 5 displays the correlation between the transition dipole moment vectors obtained by TD-DFTB and ab initio TD-DFT calculations. An excellent correlation can be seen between the two methods, and from the results shown in Table 2 we observe a good correspondence between the calculated and the experimental values. For the cases in which the experimental value has been extrapolated to vacuum the agreement of TD-DFTB prediction is correct to about 10%, whereas the TD-DFT results exhibit less accuracy. Both calculations predict the correct ordering in the cross sections.

A deeper understanding of the nature of the excitation can be obtained from the time dependent molecular orbital populations following a laser excitation in tune with the excitation energy. These populations can be obtained by rotation of the one electron time-dependent density matrix to the molecular orbital basis. The diagonal elements of this rotated density matrix represent instantaneous molecular orbital populations. Continuous laser excitation produces a coherent evolving state that is a superposition of ground and excited states and not a pure excited state; however, important information can be obtained from the instantaneous populations. Figure 6 shows the time dependent molecular orbital populations for BChla (left) and BChle (right) when a continuous laser type perturbation is applied. We have chosen to include figures here only for this pair because they have the largest and lowest transition dipole moments, respectively, for the whole explored series of pigments. The coherent and time evolving superposition of states that results from continuous laser excitation is revealed by the oscillatory nature of the populations.

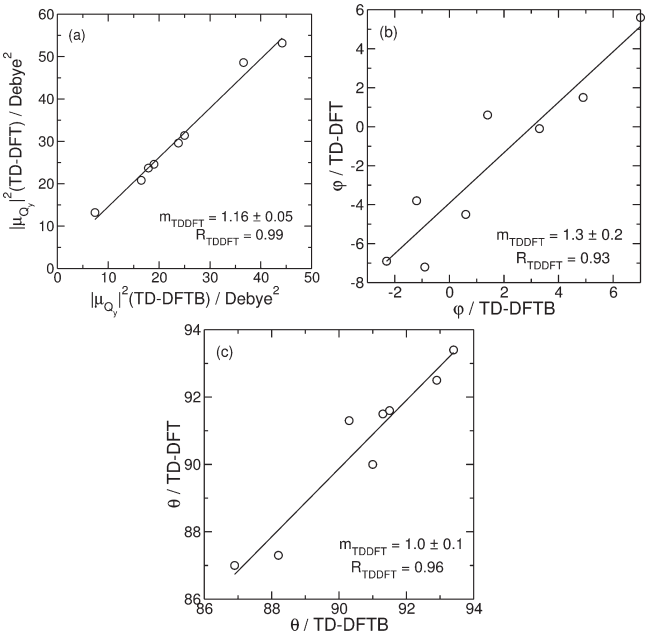

Figure 5. Correlation between the transition dipole moment vectors obtained by TD-DFTB and TD-DFT methods: (a) transition dipole moment magnitude; (b) ϕ angle; (c) θ angle. Straight lines are the linear regressions of the data; slope (m) and correlation coefficient (R) values for these regressions are also shown in the figure.

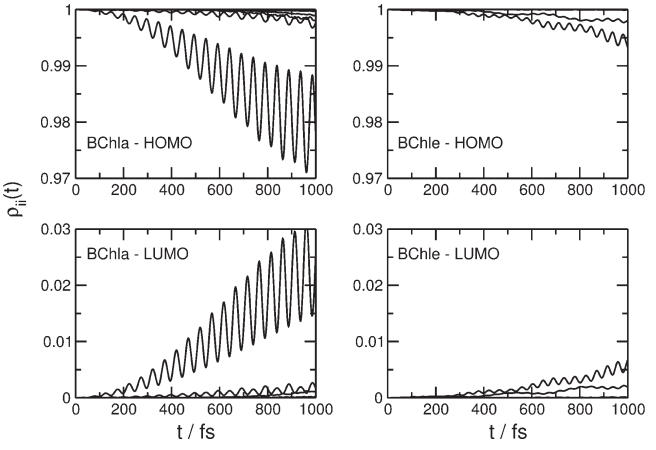

Figure 6. Time dependent transition probability of BChla (left) and BChle (right) in response to a laser illumination in tune with the Q_y electronic transition.

The vast majority of populations remain at their ground state values but some molecular orbitals change their population and a clear transfer of population can be seen from the occupied to the unoccupied manifold. Population transfer at short times has a quadratic behavior that can be expected from the application of the Fermi golden rule, which later evolves out of the simple first-order description. The largest changing populations in all cases correspond to the highest occupied molecular orbital (HOMO) and the lowest unoccupied molecular orbital (LUMO) for each molecule. The dipole strength of the excitation is revealed from the change in oscillation amplitude and the population evolution with time, which is greater for the BChla than for BChle molecule due to the large differences in cross sections, as shown in Table 2.

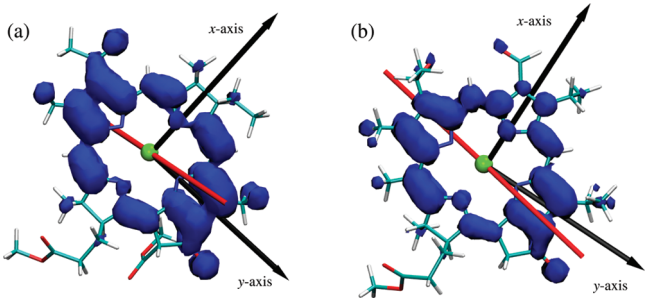

Figure 7. Transition probability density of (a) BChla and (b) BChle. Displays the *xy* plane and the direction of the Q_y electronic transition (red line).

The excitations are, however, not pure HOMO−LUMO transitions and other orbitals are involved as well. In the case of BChle only two other orbitals participate in the excitation; these are the HOMO−1 and LUMO+1, which are clearly as important as the HOMO and the LUMO in this case. In the case of BChla a larger manifold of orbitals shows evolving populations, the largest changes in population are still those corresponding to HOMO−1 and LUMO+1 orbitals. The broader manifold of orbitals that participate in the case of BChla can be explained from the fact that due to its larger transition dipole moment the local field generated inside the molecule is stronger and this local field can excite other pairs from multipolar coupling. For all the studied pigments the time evolving populations can be mapped as either similar to BChla or to BChle and this fact seems to be related to the dipole strength of the excitation. This complexity can only be expected to increase whenever excitonic coupling between closely placed pigments is involved within light harvesting complexes that are influenced by highly inhomogeneous local fields. We believe that the detailed picture provided for these excitations by the study of a fully atomistic picture can be of great value when it can be extended to the description of coupled excitations within antenna complexes, which the simplicity of the method allows. These simulations are currently underway and will be the subject of a following publication.

To shed light on the reasons for the differences observed in the magnitudes of the transition dipole moments of the Q_y excitations in different pigments, we can take into account that the main component of these excitations is a promotion of electron population from the HOMO to the LUMO and try to produce a picture of the transition density under this approximation. In a simple non-self-consistent model, the transition dipole density can be depicted in a graphical way from the function:

$$\begin{aligned}\rho(x,y,z) = {} & |\phi_{\mathrm{HOMO}}(r)|x|\phi_{\mathrm{LUMO}}(r)|^2 \\ & + |\phi_{\mathrm{HOMO}}(r)|y|\phi_{\mathrm{LUMO}}(r)|^2 \\ & + |\phi_{\mathrm{HOMO}}(r)|z|\phi_{\mathrm{LUMO}}(r)|^2 \end{aligned} \quad (6)$$

which is basically a spatially weighted projection between HOMO and LUMO orbitals. The reason for the difference in magnitude of the transition dipole moment between BChla and BChle molecules can be seen in the transition probability density (Figure 7), which for the first molecule is greater. This is revealed from the larger enclosed volume by the isosurfaces which in both figures is drawn at the same function value. The BChla can be seen to have a larger spatial extent than the one for BChle. As mentioned before, these two pigments represent the extrema of highest and lowest dipole transition strengths that we observed among the studied pigments and is therefore revealing. Besides the larger enclosed volume for the BChla isosurfaces the largest spatial extent of the transition density is clearly shown in the plots of Figure 7. An important difference is the involvement of the ketone group at position R3 in the BChla molecule meanwhile the BChle molecule has an alcohol group in that substituent for which no density can be observed at this level. The presence of the ketone group extends the conjugation outside the porphyrin ring, an effect that is absent in BChle. In addition, the BChla molecule has excitation density extending to the σ bonds in the methyl group in R12, which we can interpret as due to hyperconjugation. This effect is reduced for BChle due to the fact that there is an ethyl group in that position. Another molecule that has a large transition dipole moment is BChlb; this molecule also has a ketone group in the substituent R3, the difference with BChla is the presence of a group $=CH—CH_3$ at R8, which has a lower hyperconjugation effect. The other photosynthetic pigments that we have studied differ from these two molecules in that ring B is oxidized, which one could expect would increase conjugation in the porphyrin ring, and therefore give a higher transition dipole moment, but these molecules have a different substituent group in R3, such as an aldehyde group in Chld, an ethylene in Chla, and an alcohol group in BChlc and BChld. The effect on the extension of the conjugation of the π system out of the porphyrin ring of these groups is lower, and we think this is the most important factor, as it basically explains the order of all the calculated dipole strengths.

CONCLUSIONS

In this paper we have shown results for the calculated values of the Q_y transition dipole moments for different photosynthetic pigments and its spatial directions referred to molecular axes. These results are obtained from time propagation of the equation of motion of the one electron density matrix within the DFTB framework under the influence of external time dependent electric fields. Excellent agreement of transition dipole moments with ab initio TD-DFT and experimental results extrapolated to vacuum is observed. Transition directions are also obtained because these, together with dipole strengths, are an essential ingredient of approximate Hamiltonians used to describe coupled excitation in simpler schemes that are able to treat larger systems and involve dissipation and decoherence into the environment. We have obtained a complex albeit clear picture of the main molecular orbitals involved in the excitation outside the Fermi golden rule scope and the main chemical features of pigments that regulate the strength of the Q_y transition by identifying substituents R3 and R12 as playing important roles together with reduction of the B ring. As mentioned in the text, we are extending the model to be able to describe the coupled excitations of chromophore aggregates within light harvesting complexes from an atomistic point of view that will provide new insights into the complexities involved in multichromophore couplings that go further than simple dipole−dipole couplings. These results will be the subject of further publications.

AUTHOR INFORMATION

Corresponding Author

*E-mail: cgsanchez@fcq.unc.edu.ar.

■ ACKNOWLEDGMENT

We acknowledge support by Consejo Nacional de Investigaciones Cientficas y Técnicas (CONICET) through grants PIP 112-200801-000983 and ANPCYT through grant Program BID 1728/OC-AR PICT No 629. All calculations were performed with a generous time allocation on the *Cristina* supercomputer built with funding provided by ANPCYT through grant PME-2006-01581. M.B.O. is grateful for a studentship from CONICET. We thank Prof. Marcus Elstner for the provision of DFTB+ Slater-Koster tables for magnesium containing molecules from ref 24 and the corresponding reference densities. We are also grateful to an anonymous referee for his/her important suggestions.

■ ADDITIONAL NOTE

[†] These results were obtained with the B3PW91 functional and a 6-31+G(d) basis set as implemented in the Gaussian 09 program package[21] at the DFTB optimized geometry.

■ REFERENCES

(1) Blankenship, R. E. *Molecular Mechanisms of Photosynthesis*; Blackwell Science Ltd.: Oxford, U.K., 2002.

(2) Engel, G. S.; Calhoun, T. R.; Read, E. L.; Ahn, T.-K.; Mančal, T.; Cheng, Y.-C.; Blankenship, R. E.; Fleming, G. R. *Nature* **2007**, *446*, 782–786.

(3) Lee, H.; Cheng, Y.-C.; Fleming, G. R. *Science* **2007**, *316*, 1462–1465.

(4) Ishizaki, A.; Fleming, G. R. *Proc. Natl. Acad. Sci. U. S. A.* **2009**, *106*, 17255–17260.

(5) Adolphs, J.; Renger, T. *Biophys. J.* **2006**, *91*, 2778–2797.

(6) Olbrich, C.; Kleinekathöfer, U. *J. Phys. Chem. B* **2010**, *114*, 12427–12437.

(7) Hsin, J.; Strümpfer, J.; Sener, M.; Qian, P.; Hunter, C. N.; Schulten, K. *New J. Phys.* **2010**, *12*, 085005–085025.

(8) Oviedo, M. B.; Negre, C. F. A.; Sanchez, C. G. *Phys. Chem. Chem. Phys.* **2010**, *12*, 6706–6711.

(9) Fragata, M.; Nordén, B.; Kurucsev, T. *Photochem. Photobiol.* **1988**, *47*, 133–143.

(10) Linke, M.; Lauer, A.; von Haimberger, T.; Zacarias, A.; Heyne, K. *J. Am. Chem. Soc.* **2008**, *130*, 14904–14905.

(11) Linke, M.; Theisen, M.; von Haimberger, T.; Madjet, M. E.; Zacarias, A.; Fidder, H.; Heyne, K. *Chem. Phys. Chem.* **2010**, *11*, 1283–1288.

(12) Elstner, M.; Porezag, D.; Jungnickel, G.; Elsner, J.; Haugk, M.; Frauenheim, T.; Suhai, S.; Seifert, G. *Phys. Rev. B: Condens. Matter Mater. Phys.* **1998**, *58*, 7260–7268.

(13) Yabana, K.; Bertsch, G. F. *Phys. Rev. B: Condens. Matter Mater. Phys.* **1996**, *54*, 4484–4487.

(14) Castro, A.; Appel, H.; Oliveira, M.; Rozzi, C. A.; Andrade, X.; Lorenzen, F.; Marques, M. A. L.; Gross, E. K. U.; Rubio, A. *Phys. Status Solidi B* **2006**, *243*, 2465–2488.

(15) Georgakopoulou, S.; van der Zwan, G.; Bassi, R.; van Grondelle, R.; van Amerongen, H.; Croce, R. *Biochemistry* **2007**, *46*, 4745–4754.

(16) Kleima, F. J.; Hofmann, E.; Gobets, B.; van Stokkum, I. H.; van Grondelle, R.; Diederichs, K.; van Amerongen, H. *Biophys. J.* **2000**, *78*, 344–353.

(17) Cai, Z.-L.; Crossley, M. J.; Reimers, J. R.; Kobayashi, R.; Amos, R. D. *J. Phys. Chem. B* **2006**, *110*, 15624–15632.

(18) Mukamel, S. *Principles of Nonlinear Optical Spectroscopy*; Oxford University Press, Inc.: New York, 1995.

(19) Knox, R. S. *Photochem. Photobiol.* **2003**, *77*, 492–496.

(20) Knox, R. S.; Spring, B. Q. *Photochem. Photobiol.* **2003**, *77*, 497–501.

(21) Frisch, M. J.; Trucks, G. W.; Schlegel, H. B.; Scuseria, G. E.; Robb, M. A.; Cheeseman, J. R.; Scalmani, G.; Barone, V.; Mennucci, B.; Petersson, G. A.; Nakatsuji, H.; Caricato, M.; Li, X.; Hratchian, H. P.; Izmaylov, A. F. et al. *Gaussian 09*, Revision A.01; Gaussian, Inc.: Wallingford, CT, 2009.

(22) Warshel, A.; Parson, W. W. *J. Am. Chem. Soc.* **1987**, *109*, 6143–6152.

(23) Hughes, J. L.; Razeghifard, R.; Logue, M.; Oakley, A.; Wydrzynski, T.; Krausz, E. *J. Am. Chem. Soc.* **2006**, *128*, 3649–3658.

(24) Cai, Z.-L.; Lopez, P.; Reimers, J. R.; Cui, Q.; Elstner, M. *J. Phys. Chem. A* **2007**, *111*, 5743–5750.